Layering in Crumpled Sheets

by

David Aristoff and Charles Radin

Mathematics Department, University of Texas, Austin, TX 78712

Abstract

We introduce a toy model of crumpled sheets. We use simulation to show there is a first order phase transition in the model, associated with an abrupt initiation of layering as confinement is increased.

December, 2009

1. Introduction.

When a sheet of stiff paper is crumpled into a compact ball, creases and folds appear. In particular, creases are produced corresponding to irreversibly distorted material, and some of the energy expended in confining the material becomes concentrated in them. The creases constitute a very small fraction of the volume of the material, so the energy is being stored very inhomogeneously. This has been widely studied, for instance in [1,2,3]. Our interest here is in an analogous geometric inhomogeneity, associated with the folds, which is less well understood due to the difficulty of determining the effect of excluded volume. See for instance [4,5].

Consider the densest possible state of the material, in which the sheet is carefully folded into a compact stack of parallel leaves. (There needs to be a significant cost for bending and creasing the material, or else dense packings will usually be more complicated. This is discussed in section 3.) Imagine the process of compactifying the sheet within a contracting sphere, from a typical initial state of low volume fraction near 0 to a typical state of high volume fraction near 1. One can ask how such a process would proceed. For a material in thermal equilibrium there is a first order phase transition associated with quasistatic compactification; low density configurations are of random character (fluid), while high density configurations are ordered (solid), and isothermal compactification would progress between the extremes via freezing and melting transitions, separated by phase coexistence in which the material consists of macroscopic portions of each phase. Our computations, in a toy model, suggests that compactification of stiff sheets undergoes a similar path from its low volume fraction disordered states to its high volume fraction ordered states, making use of a reorganization of the state into an inhomogeneous intermediary as is typical of freezing.

Consider configurations of a thin, stiff sheet of volume v confined within a volume V. We will model the stiffness of the sheet by a form $\mathcal{E}(C)$ for the total energy of bends and creases in configuration C. Then let $\mathcal{A}_V(v,\mathcal{E})$ be the set of all possible configurations in V of volume v and energy $\mathcal{E}$, and let $\mathbb{Z}_V(v,\mathcal{E})$ be the volume of $\mathcal{A}_V(v,\mathcal{E})$. Finally let $\phi = v/V$ be the volume fraction, $u = \mathcal{E}/V$ be the energy density, and $s(\phi,u) = \lim_{V\to\infty} \ln[Z_V(v,\mathcal{E})]/V$ be the exponential rate of growth of $\mathbb{Z}_V(v,\mathcal{E})$, where the infinite volume limit is taken with fixed ϕ and u. $s(\phi,u)$ will play the role of a free energy in our model. We will give (indirect) evidence that $s(\phi,u)$ has a flat portion in its graph, corresponding to phase coexistence between a disordered, low volume fraction/high energy phase and an ordered, folded, high volume fraction/low energy phase. The folding is accompanied by a spontaneous breaking of symmetry in which the elements of the sheet have a preferential normal direction.

Our toy model is not of a thin, stiff sheet in 3 dimensions but of a thin, stiff wire loop in 2 dimensions, which we expect to behave similarly [6]. And in the model the wire is restricted to the edges of a triangular lattice.

2. The Model, and Results.

For fixed integer n consider the triangular lattice $L = \{(a + b/2, b\sqrt{3}/2) : (a,b) \in (\mathbb{Z}/n\mathbb{Z})^2\}$ with periodic boundary conditions. Note that this space is homogeneous

and isotropic. (We will also consider hard wall boundaries.)

Let $\mathcal{A}$ be the set of connected, self-avoiding cycles (oriented loops) with vertices in L and edges of unit length. (See Figure 1.) If the edges meeting at a vertex form a nonzero angle we say there is a *bend* at that vertex. We associate an energy $\mathcal{E}_3(b)$ with any bend b of angle $\pm\pi/3$ and an energy $\mathcal{E}_6(b)$ with any bend of angle $\pm\pi/6$. We call an element of $\mathcal{A}$ a *configuration*.

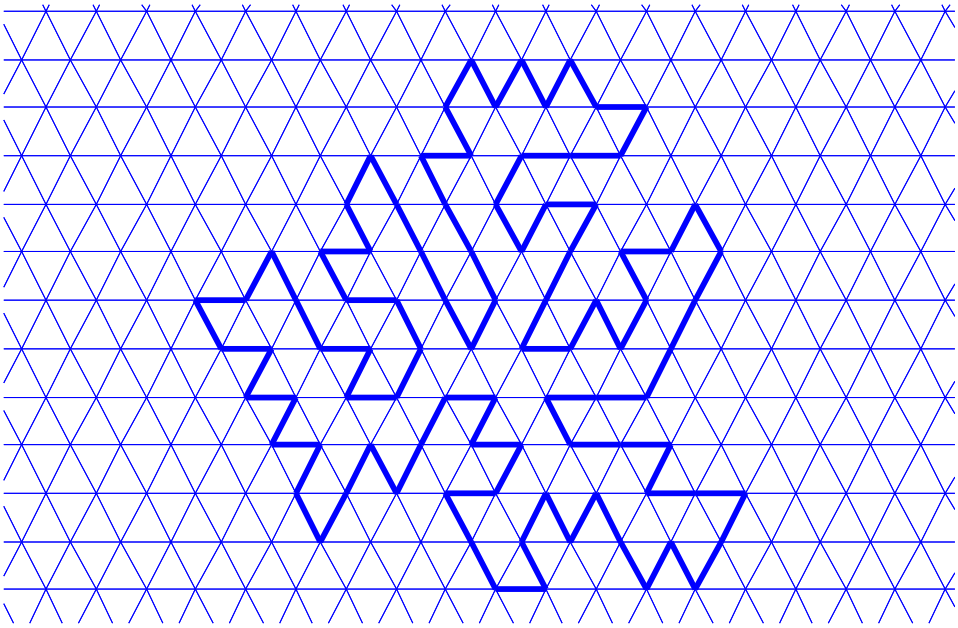

Figure 1. A loop.

Because it is harder to simulate our model at fixed density and/or fixed energy, we introduce the conjugate variables β for energy $\mathcal{E}$ and μ for particle number N, assigning the probability $m_\mu(C)$ for any $C \in \mathcal{A}$:

$$m_\mu(C) = \frac{e^{-\beta[\mathcal{E}(C)-\mu N(C)]}}{Z}, \tag{1}$$

where Z is the normalization. (We suppress dependence on the system size.) So there are 3 variables in our model: μ, β, and the ratio of the energies of the two bending angles.

We consider two variants for the energy $\mathcal{E}(C)$:

$$\mathcal{E}(C) = \sum_{b \in C} [\mathcal{E}_3(b) + \mathcal{E}_6(b)]. \tag{2}$$

One variant uses: $\mathcal{E}_6(b) = 2$ for bends b of angle $\pi/6$ and 0 otherwise, and $\mathcal{E}_3(b) = 1$ for bends of angle $\pi/3$ and 0 otherwise. The other variant uses: $\mathcal{E}_6(b) = +\infty$ for bends of angle $\pi/6$ and 0 otherwise, and $\mathcal{E}_3(b) = 1$ for bends of angle $\pi/3$ and 0 otherwise. We use the shorthand $1:2$ to refer to the former model, and $1:\infty$ to refer to the latter.

It is difficult to simulate this model at high μ (or high volume fraction) so we fix $\beta = 1$ and vary μ starting from low values. We run Markov chain Monte Carlo simulations as follows. We first pick a mesh $\mathcal{M} = \{\mu_0, \mu_1, ..., \mu_{l-1}\}$ of μ values $\mu_0 < \mu_1 < ... < \mu_{l-1}$. For each μ_i we use a protocol $\mathcal{P}_i$ which allows us to sample from μ_i; that is, given any initial configuration, the protocol $\mathcal{P}_i$ generates a Markov chain with stationary measure m_{μ_i}. The basic step in the protocol is the following. From a given configuration $C \in \mathcal{A}$, we choose a random subpath σ_d of length d. We then consider all configurations $C' \in \mathcal{A}$ obtainable from C by replacing σ_d with a path $\sigma_{d'}$ while leaving the rest of C unchanged. Here σ_d and $\sigma_{d'}$ have the same endpoints and the length d' of $\sigma_{d'}$ is bounded, $d_1 \leq d' \leq d_2$. We then choose $C' \in \mathcal{A}$ with acceptance probabilities determined by m_{μ_i} as usual in Markov chain Monte Carlo [7-10]. For the $1 : \infty$ model we take $d = 5$, $d_1 = 1$ and $d_2 = 9$. For the $1 : 2$ model we choose, with probability 0.5, either $d = 1$ and $d_1 = d_2 = 2$, or $d = 2$ and $d_1 = d_2 = 1$.

Our starting configuration C_0 when simulating μ_0 is a cycle consisting of 6 edges. We aim to have some number k of samples from each m_{μ_i}, where k is chosen by a mixing time criterion which we describe below. In practice $m_{\mu_{i+1}}$ is not much larger than m_{μ_i}, and we create our samples by using the ending configuration in the simulation of μ_i as the initial configuration in the simulation of μ_{i+1}, thereby generating a chain $\mathcal{S} = (C_1, C_2, ..., C_{kl})$ of configurations. In summary, for each $i = 0, 1, ..., l$, we take k Monte Carlo steps starting from configuration C_{ki}, such that the steps are performed according to the protocol $\mathcal{P}_i$ described above, to get configurations $C_{ki+1}, C_{ki+2}, ..., C_{ki+k}$. We call $(C_{ki+1}, C_{ki+2}, ..., C_{ki+k})$ the *subchain* $\mathcal{S}_i$ corresponding to μ_i. The full chain $\mathcal{S} = (\mathcal{S}_0, ..., \mathcal{S}_{l-1})$ can be thought of as the sequential collection of its l subchains, each of which simulates one of the selected μ_i.

For each subchain $\mathcal{S}_i = (C_{ki+1}, C_{ki+2}, ..., C_{ki+k})$, we take measurements which might detect the spontaneous symmetry breaking, and layering, which we expect to occur at large μ. We first consider a correlation measurement $corr(C)$, which we perform as follows: choose a random edge e in C and take $corr(C)$ to be the proportion of edges in C which are parallel to e. The measurement $corr$ should be able to detect broken symmetry; in particular since the model is isotropic, we expect that $corr(\mu)$ should be identically $1/3$ for small μ in the infinite volume limit.

Next we take a measurement to detect bulk-sized layers; that is, layers that are proportional in size to the system volume. We let $lay(C)$ be the normalized size of the largest 80% perfect "layer" at the origin in configuration C, as follows. Recall that our model consists of oriented cycles; for an oriented edge $e = (v_1, v_2)$ we say that e *points to the vertex* v_2. Now, we let $lay(C) = 0$ if there is no edge pointing to the origin in C. Otherwise let e_0 be the edge in C pointing to the origin. Taking $g_i(C)$ to be the number of edges which are parallel to e_0 and which point to vertices in $B_i = \{(a + b/2, b\sqrt{3}/2) \in L : |a| \leq i, |b| \leq i\}$, we define $lay(C) = n^{-2} \cdot \max\{(2i+1)^2 : g_i(C) > 0.8(2i+1)^2\}$. We expect that for small μ, lay is identically zero in the infinite volume limit. Note that the choice of 80% is rather arbitrary; any percentage significantly above 33% should detect bulk-sized layers.

Finally we let $\phi(C)$ to be volume fraction, i.e., the number of edges in C divided by $n^2 - 1$. To estimate the true values of our measurements at various μ_i we make

measurements at regular intervals j on our chain of k configurations. For each subchain $\mathcal{S}_i$ we record an average measurement which corresponds to the associated measure m_{μ_i}. Specificially, for $\mathcal{S}_i = (C_{ki+1}, C_{ki+2}, ..., C_{ki+k})$ we compute the averages:

$$\phi(\mathcal{S}_i) := \tfrac{j}{k}[\phi(C_{ki+j}) + \phi(C_{ki+2j}) + ... + \phi(C_{ki+k})]$$
$$corr(\mathcal{S}_i) := \tfrac{j}{k}[corr(C_{ki+j}) + corr(C_{ki+2j}) + ... + corr(C_{ki+k})]$$
$$lay(\mathcal{S}_i) := \tfrac{j}{k}[lay(C_{ki+j}) + lay(C_{ki+2j}) + ... + lay(C_{ki+k})]$$

To determine whether k is large enough for our runs to be in equilibrium (and consequently whether the above averages are relevant), we compute "mixing times" for each of these measurements and each μ_i by using the standard autocorrelation function on each subchain $\mathcal{S}_i$. For example, if we measure autocorrelation A on $(a_1, a_2, ..., a_{k/j})$ where $a_t = \phi(C_{ki+tj})$, the mixing time M_i^ϕ is then the smallest t such that

$$A(t) := \frac{1}{b(k/j - t)} \sum_{s=1}^{k/j-t} (a_s - a) \cdot (a_{s+t} - a) < 0 \tag{3}$$

where a and b are the sample mean and variance, respectively, of $(a_1, a_2, ..., a_{k/j})$. We define M_i^{corr} and M_i^{lay} analogously. We found that our subchains had length equal to at least 20 mixing times for the $1:2$ model, and at least 50 mixing times for the $1:\infty$ model, and concluded that our runs were appropriate to simulate the μ_i. To get error bars for the measurement averages defined above we needed more data. We therefore reproduced each of our chains 200 times; that is, using the protocol for sampling the chain $\mathcal{S}$, we produce 200 independent copies of $\mathcal{S}$. We then took our measurement averages $\phi(\mathcal{S}_i)$, $corr(\mathcal{S}_i)$, and $lay(\mathcal{S}_i)$, and averaged them over the 200 copies. The latter averages we denote by ϕ_i, $corr_i$, and lay_i, respectively; we consider them to be estimates of the true volume fraction, correlation, and "80% perfect" layer density at the origin corresponding to the measure m_{μ_i}. We give evidence that these estimates are reasonable by the error bars described below.

First, we averaged the mixing times M_i^ϕ, M_i^{corr} and M_i^{lay} over the 200 copies, and found that each subchain $\mathcal{S}_i$ had length at least 20 (resp. 50) times each of the corresponding average mixing times in the $1:2$ (resp. $1:\infty$) model, as claimed above. Thus our runs are long enough to be approximately in equilibrium; furthermore, our runs are long enough for the quantities $\phi(\mathcal{S}_i)$, $corr(\mathcal{S}_i)$, and $lay(\mathcal{S}_i)$ to be approximately normally distributed. Since the 200 copies of each of these quantities are certainly independent (they come from independent copies of $\mathcal{S}$), we use Student's t-distribution to obtain 95% confidence intervals for ϕ_i, $corr_i$, and lay_i.

The data gives strong evidence of a phase transition, in the infinite volume limit, at some $\mu^* \approx -0.2$ in the $1:\infty$ version, and at some $\mu^* \approx 0.6$ in the $1:2$ version. (That the $1:2$ version undergoes a transition at a larger μ is to be expected, because making bends is less costly in that version.) If we define $corr(\mu)$ and $lay(\mu)$ as the expected values of $corr(C)$ and $lay(C)$, respectively, for C drawn from the infinite volume distribution m_μ, the data suggests that $corr(\mu)$ is identically $1/3$ for $\mu < \mu^*$ and $corr(\mu) > 1/3$ for $\mu > \mu^*$. See Figure 2 for the $1:2$ model, with error bars in Figure 3, and Figure 4 for the $1:\infty$ model, with error bars in Figure 5. As

shown, the data in Figures 2 and 4 refers to simulations made on systems of volume: $40^2 = 1600$, $60^2 = 3600$, $80^2 = 6400$ and $100^2 = 10,000$, showing well defined asymptotic limits, supporting our expectation that in the infinite volume limit there is, at some μ^*, a spontaneous breaking of symmetry, to a preferential edge direction. This phenomenon can be seen in configuration snapshots: see Figures 10-14 for the $1:2$ model and Figures 15-20 for the $1:\infty$ model, all for volume 100^2. (The correspondence between volume fraction and μ can be seen in Figures 21-22 for the two model versions.)

As further detail of the nature of the ordered phase signalled by *corr*, the data displayed in Figures 6-9, computed in the same family of simulations, suggests that in the infinite volume limit *lay* is identically zero below μ^*, but positive above μ^*. Thus we see bulk-sized layers growing above μ^*, that is, we see layered regions forming which have volume which is a positive fraction of the system volume. The spontaneous formation of bulk-sized layers above μ^* shows there is a "mixed phase" above μ^*. In a finite system, as in our simulations, this is evidenced by configurations which consist of bulk folded regions mixed with bulk unfolded regions; in the infinite system the same phenomenon would be represented by a probability distribution which is a convex combination of two "pure" distributions (states), one concentrated on folded configurations and one concentrated on unfolded configurations. We therefore believe that each version of the model undergoes a first order phase transition at its μ^*.

3. Summary.

We have introduced and simulated two versions of a 2 dimensional toy model of the folding of confined stiff sheets or wire. We find that bulk folding emerges at a sharp volume fraction as the material is compacted, analogous to the freezing transition of equilibrium fluids. This analogy has previously been used to model the behavior of other types of soft matter, in particular colloids [11] and granular matter [12,13].

We also did simulations of the $1:\infty$ version of the model with flat, hard wall boundary conditions. The transition is not as easy to see but it appears to occur at the same μ^* as with periodic boundary conditions and to have the same character, but now with folding always seeded at the boundary, as would be expected in a freezing transition. See Figures 23-24.

The folding in our model requires the use of a significant cost for bending, as we see from a typical high volume fraction simulation in Figure 25, in which such cost is absent.

The phase transition we find in our model should be experimentally verifiable, in both compacted stiff sheets and in 2 dimensionally confined compacted stiff wires.

Acknowledgements. The authors gratefully acknowledge useful discussions with W.D. McCormick, N. Menon and H.L. Swinney on the experimental possibilities of crumpled materials, and financial support from NSF Grant DMS-0700120 and Paris Tech (E.S.P.C.I.)

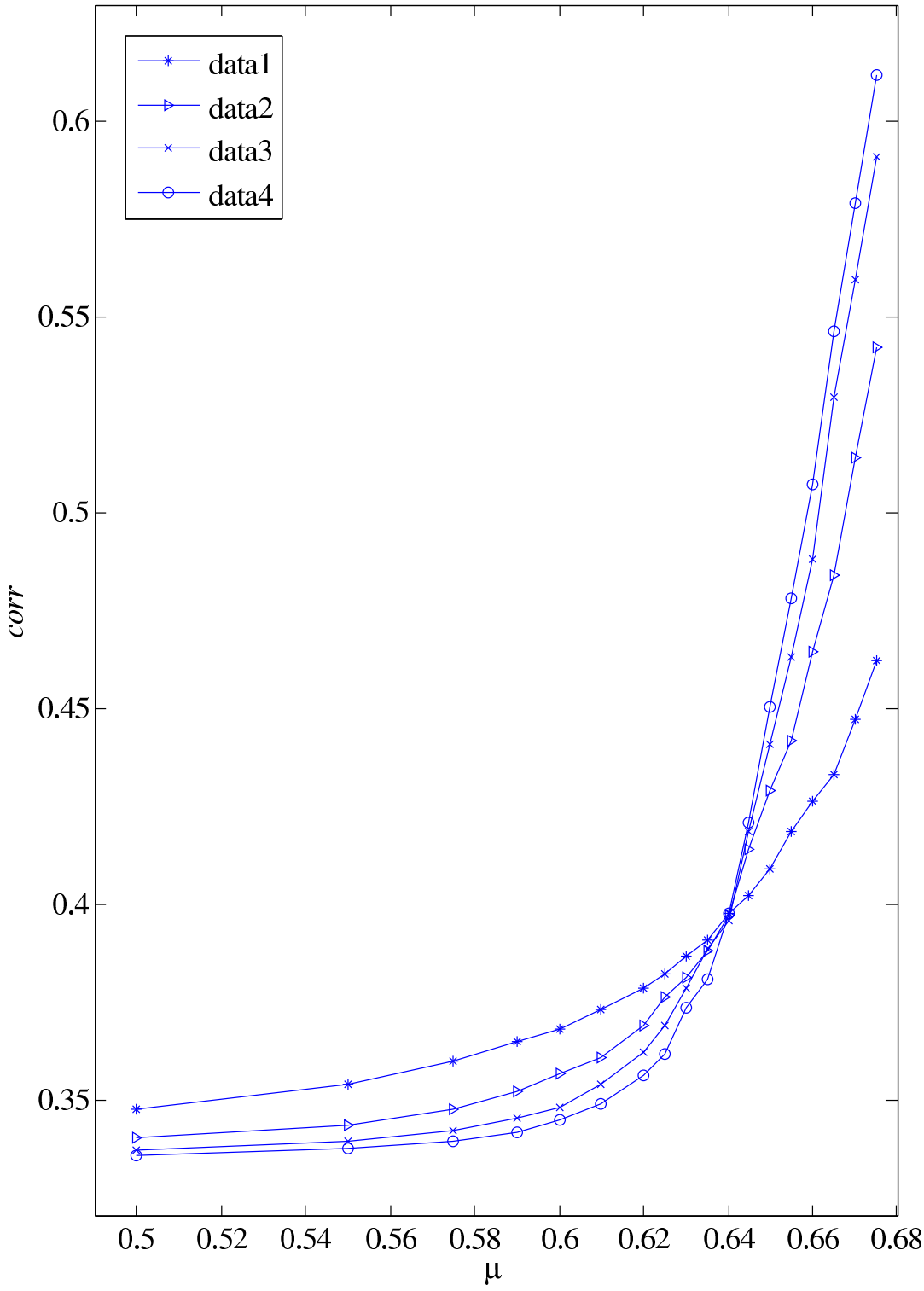

Figure 2. Correlation vs. mu for the $1:2$ model, for volumes 40^2 (data1) through 100^2 (data4).

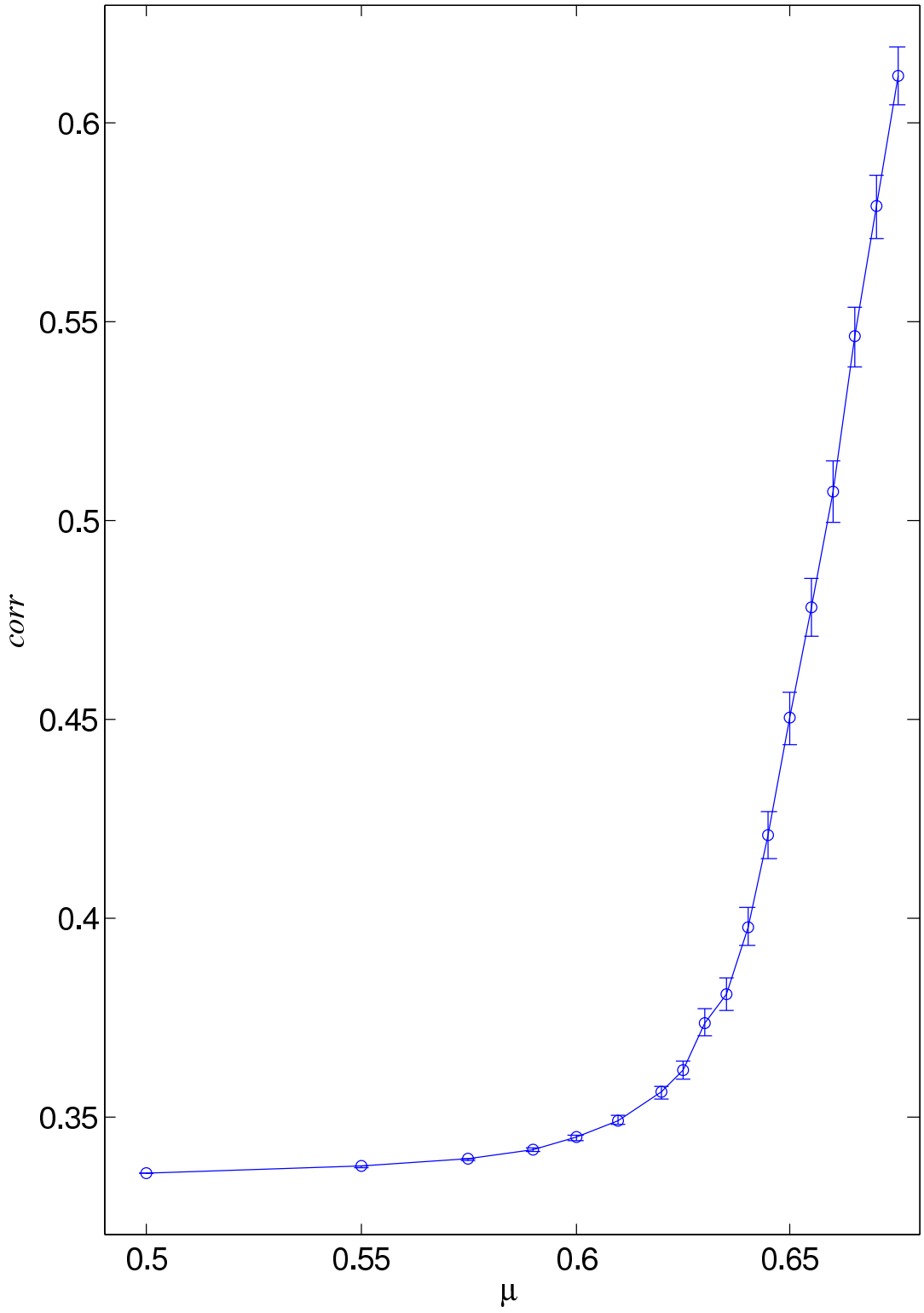

Figure 3. Correlation vs. mu for the 1 : 2 model, with errorbars, for a system of volume 100^2.

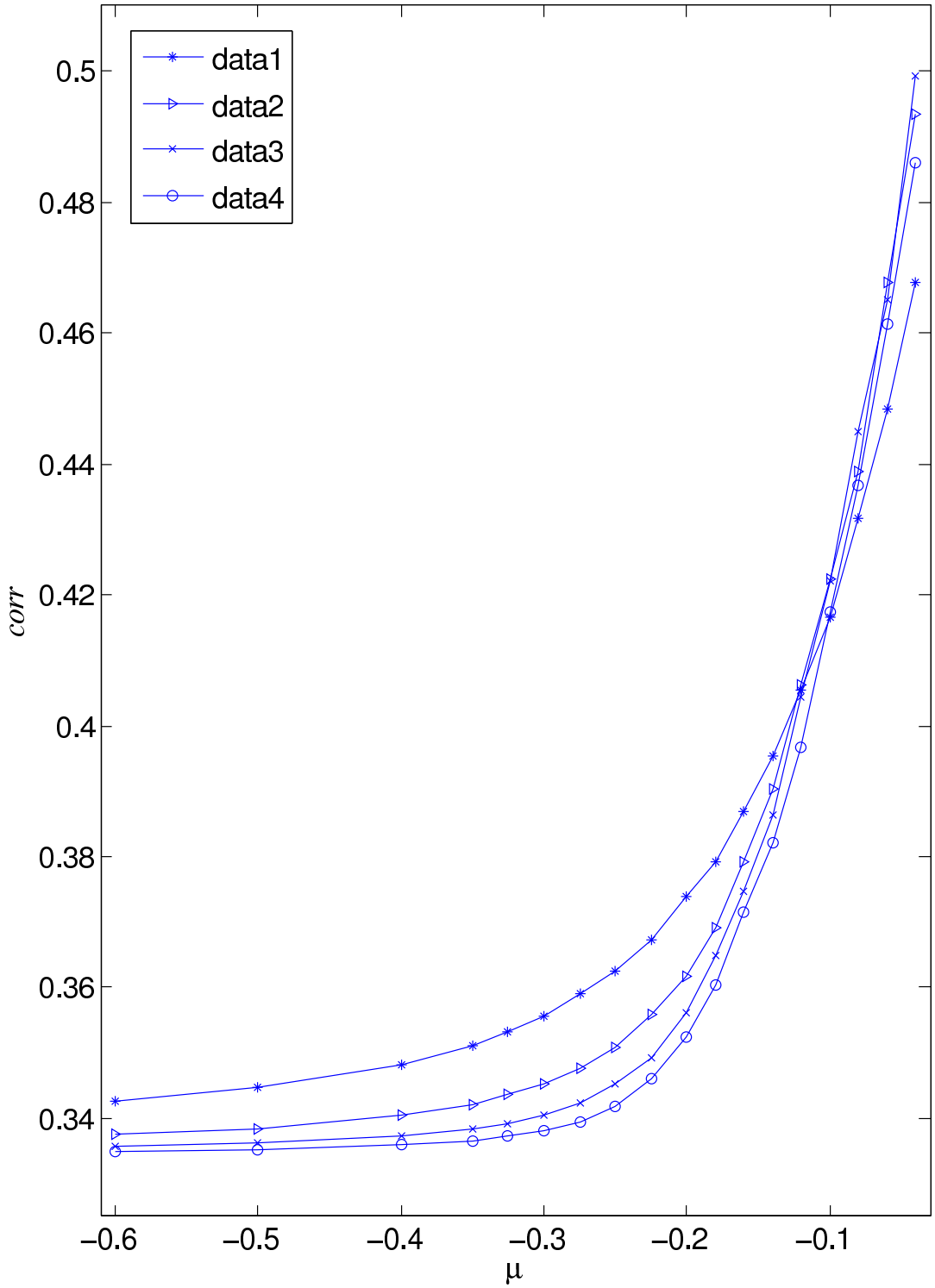

Figure 4. Correlation vs. mu for the $1 : \infty$ model, for volumes 40^2 (data1) through 100^2 (data4).

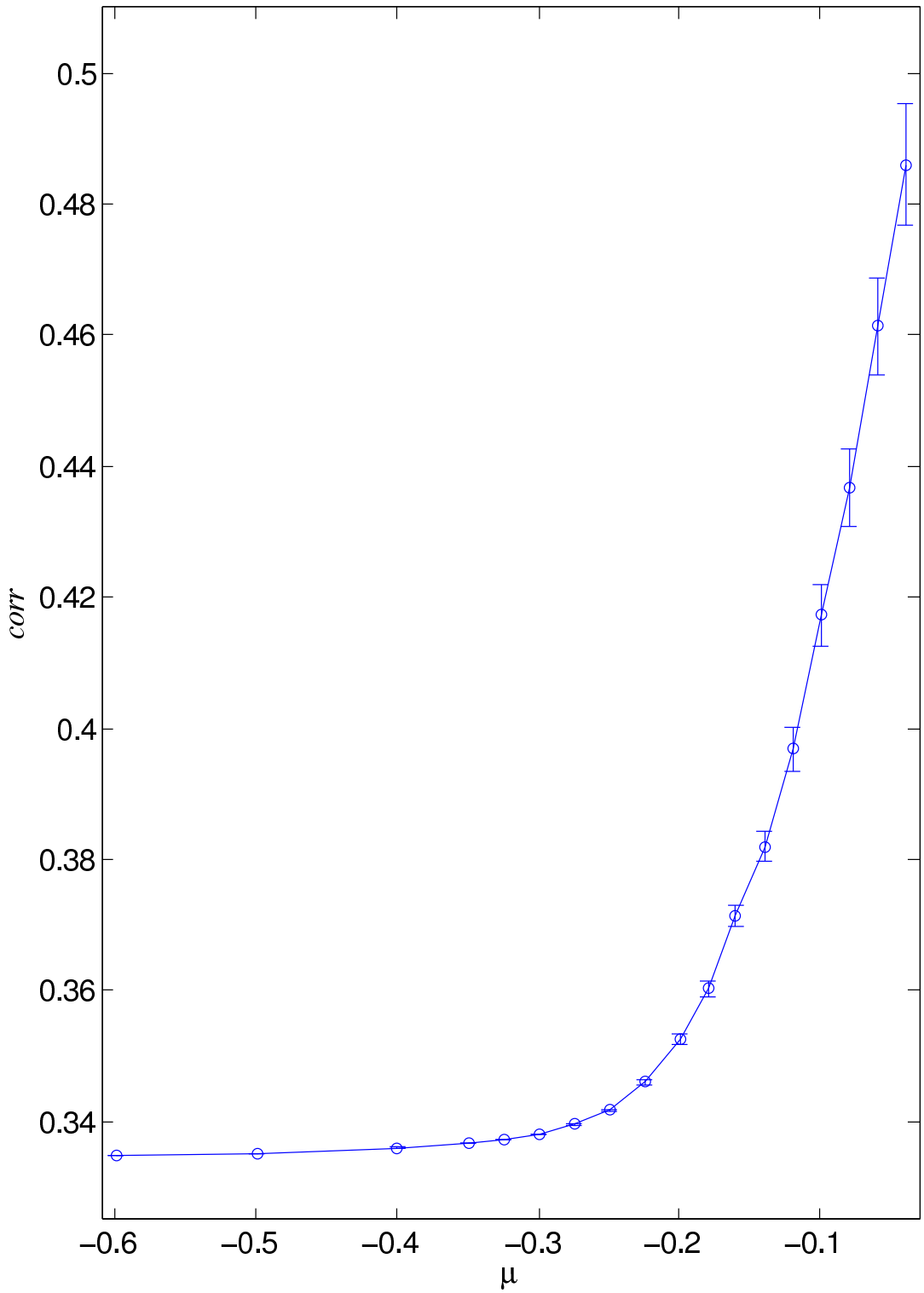

Figure 5. Correlation vs. mu for the $1 : \infty$ model, with errorbars, for a system of volume 100^2.

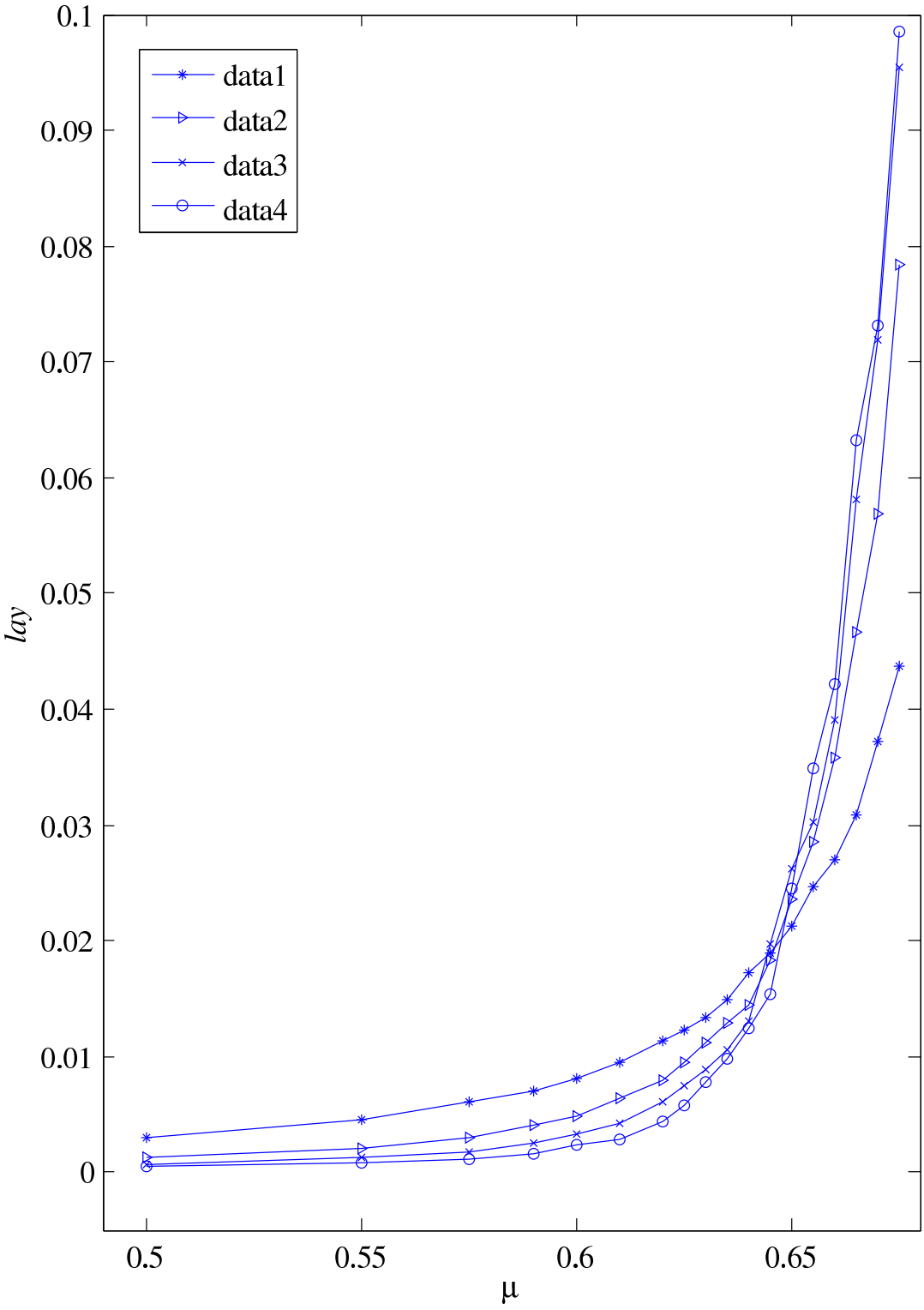

Figure 6. Layer size vs. mu for the $1:2$ model, for volumes 40^2 (data1) through 100^2 (data4).

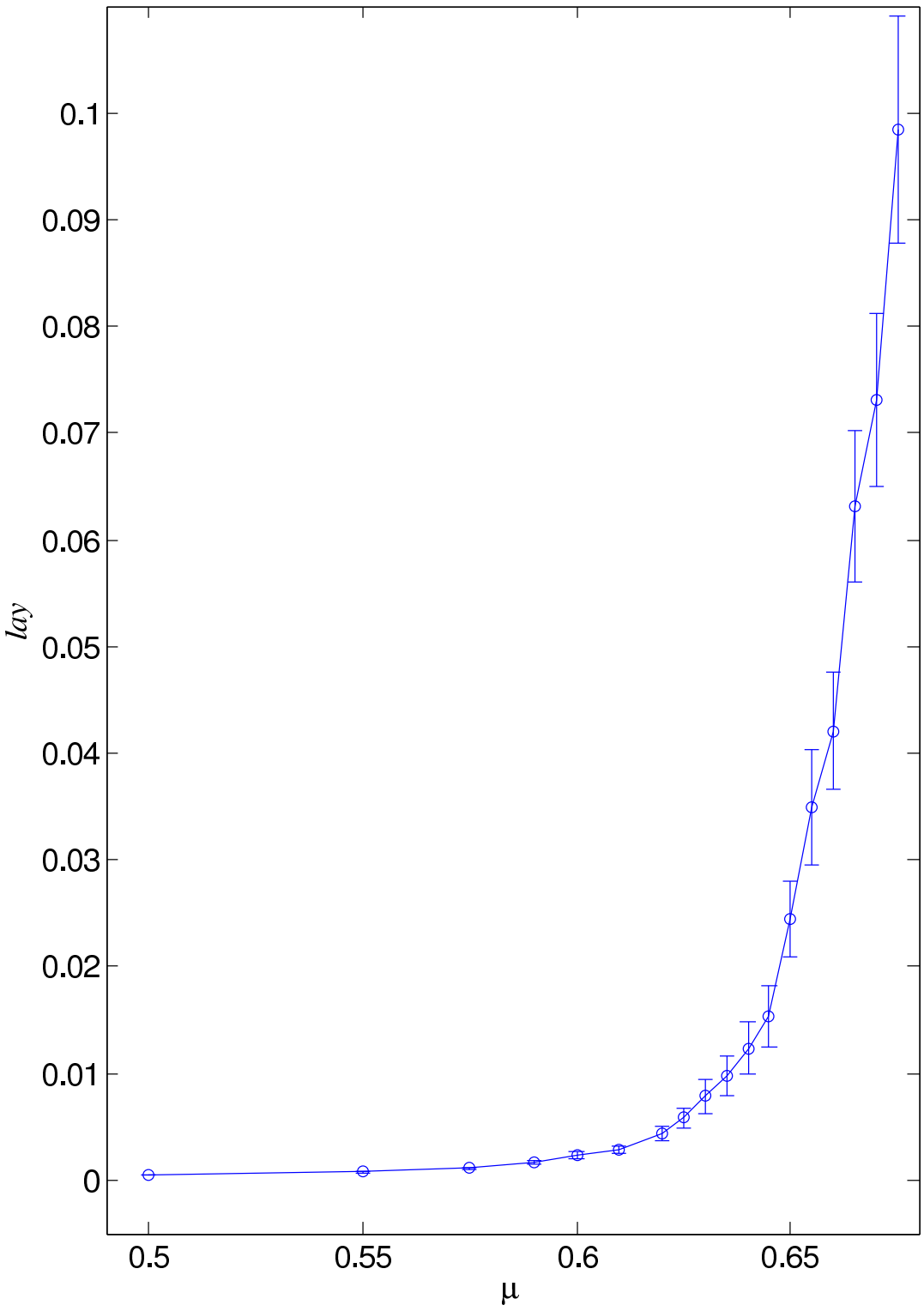

Figure 7. Layer size vs. mu for the $1:2$ model, with errorbars, for a system of volume 100^2.

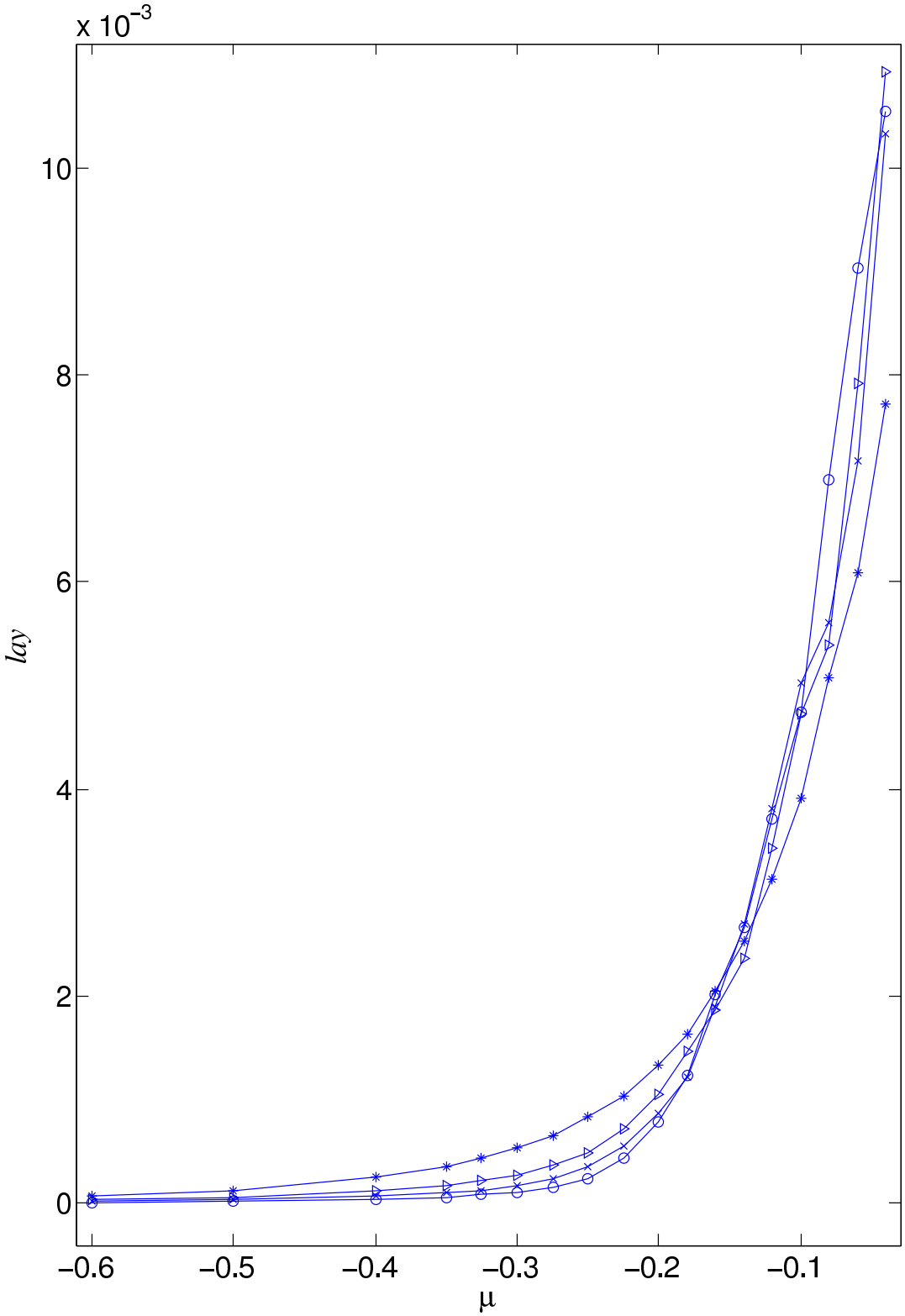

Figure 8. Layer size vs. mu for the $1 : \infty$ model, for volumes 40^2 (data1) through 100^2 (data4).

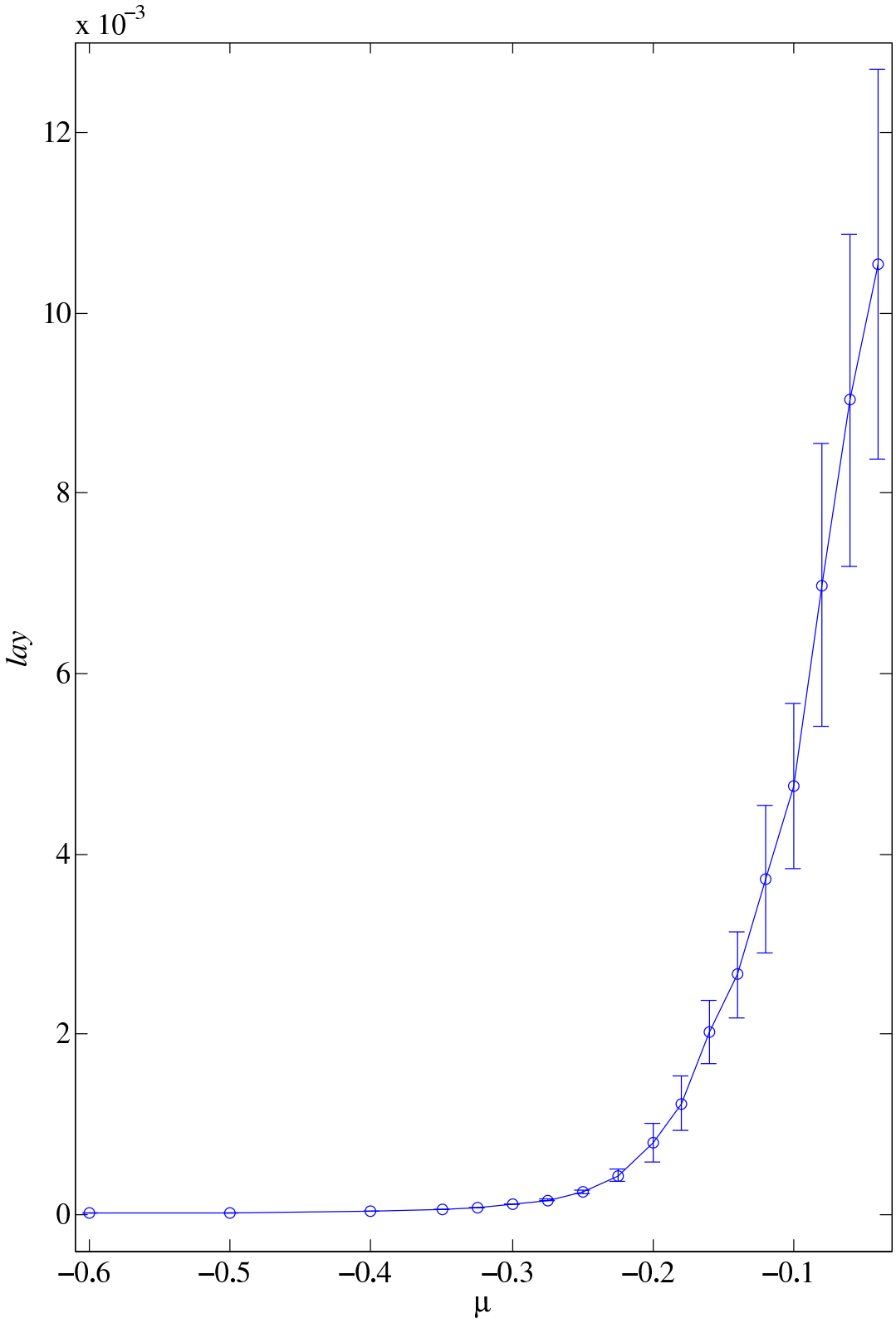

Figure 9. Layer size vs. mu for the $1 : \infty$ model, with errorbars, for a system of volume 100^2.

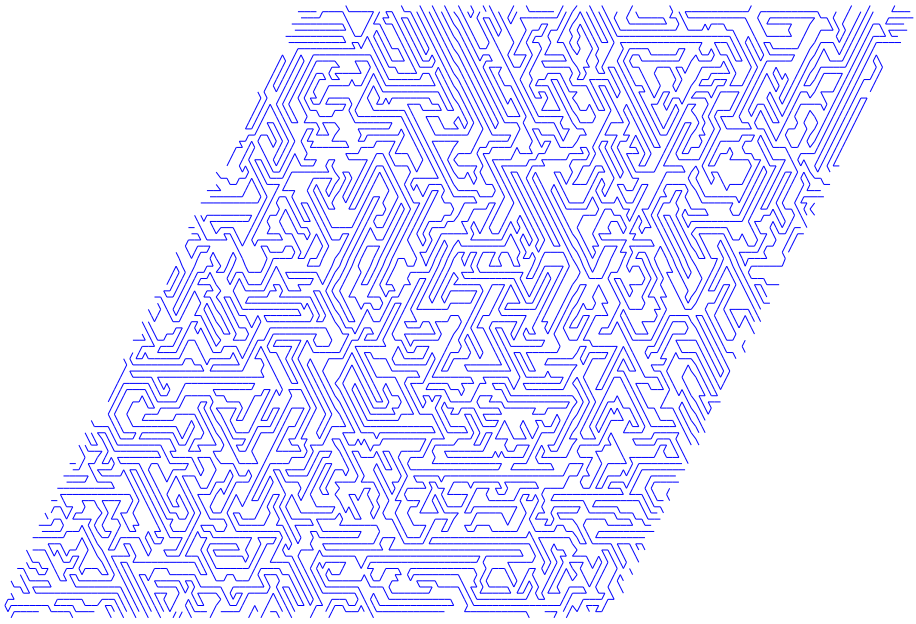

Figure 10. The $1:2$ model in equilibrium at $\mu = 0.5$

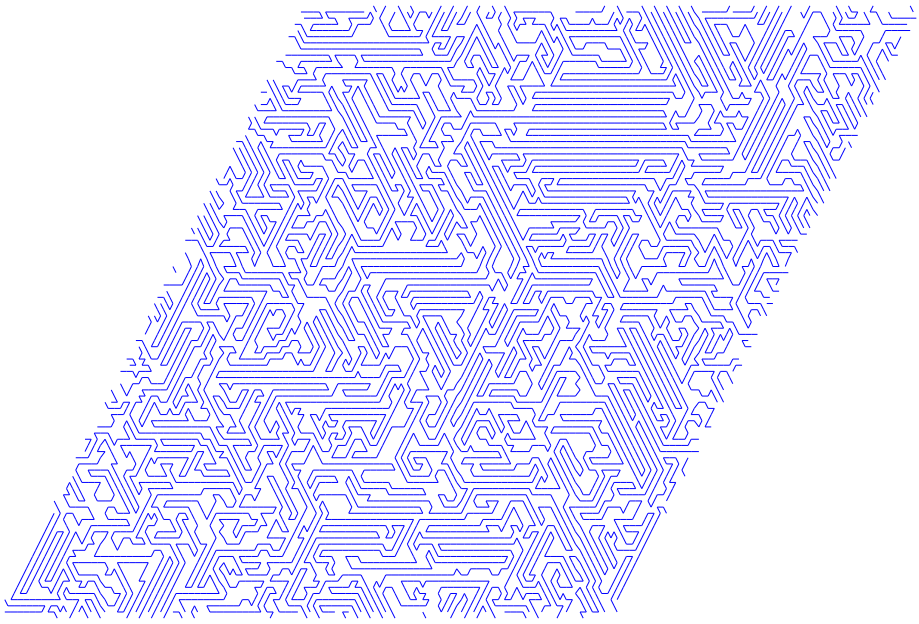

Figure 11. The $1:2$ model in equilibrium at $\mu = 0.6$

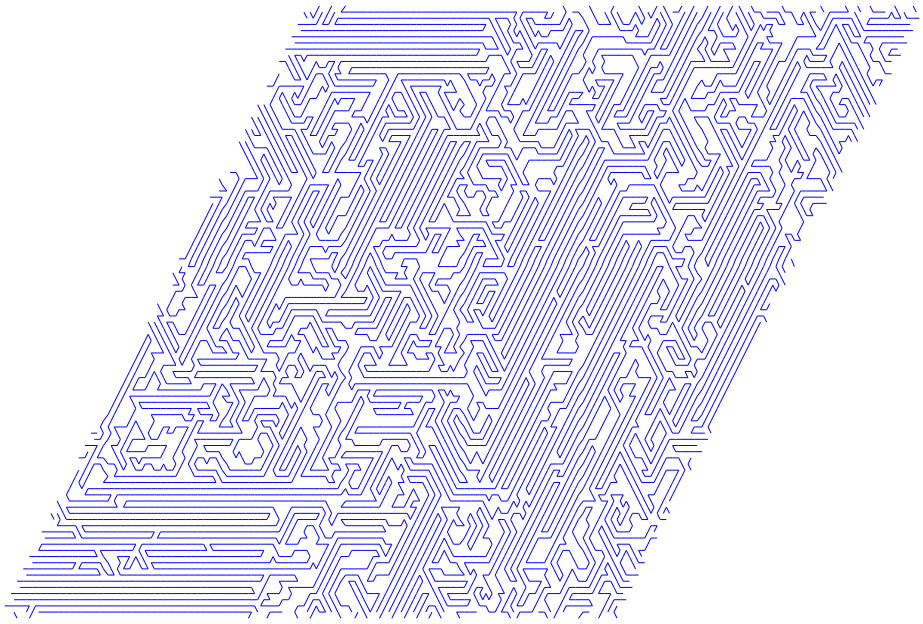

Figure 12. The $1:2$ model in equilibrium at $\mu = 0.63$

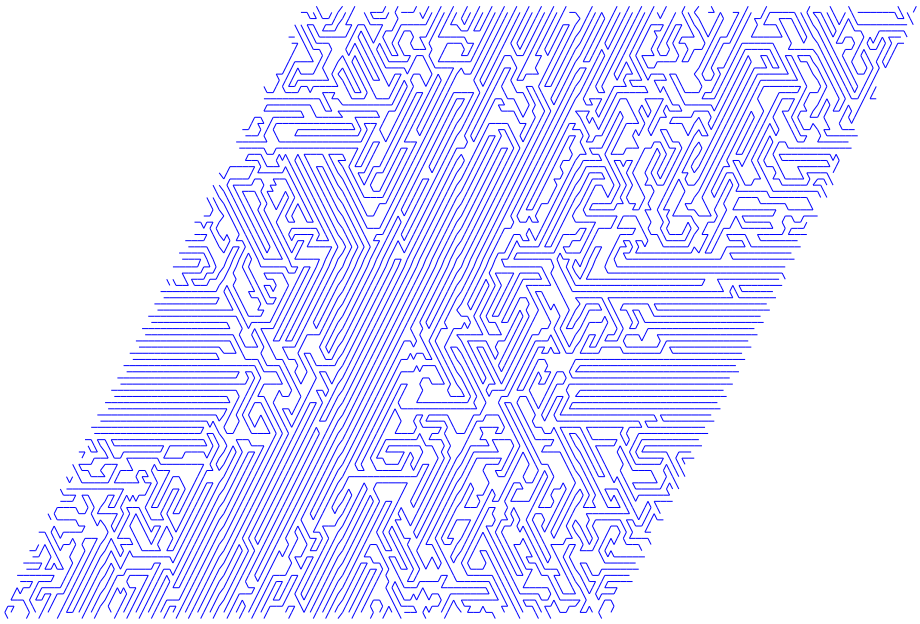

Figure 13. The $1:2$ model in equilibrium at $\mu = 0.65$

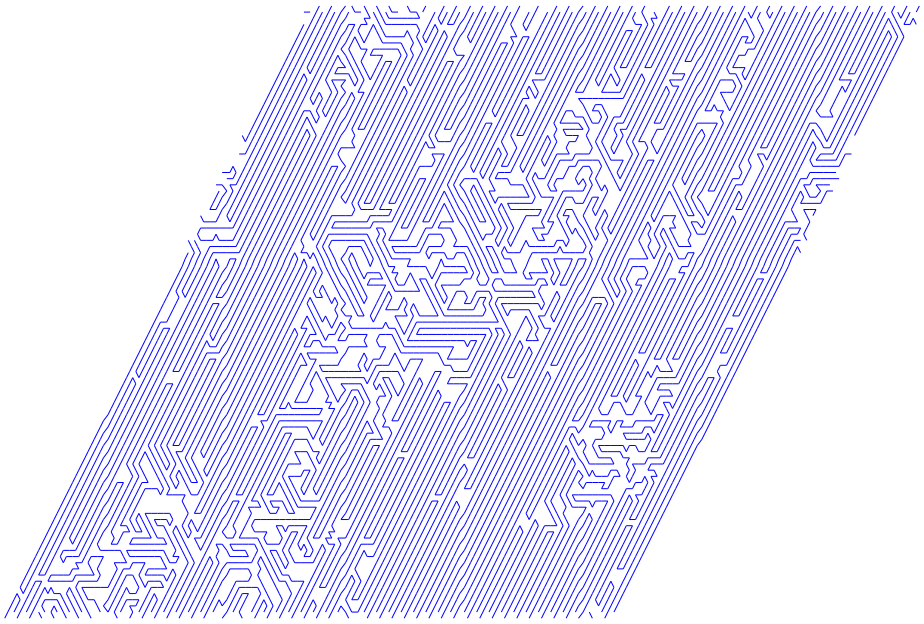

Figure 14. The $1:2$ model in equilibrium at $\mu = 0.67$

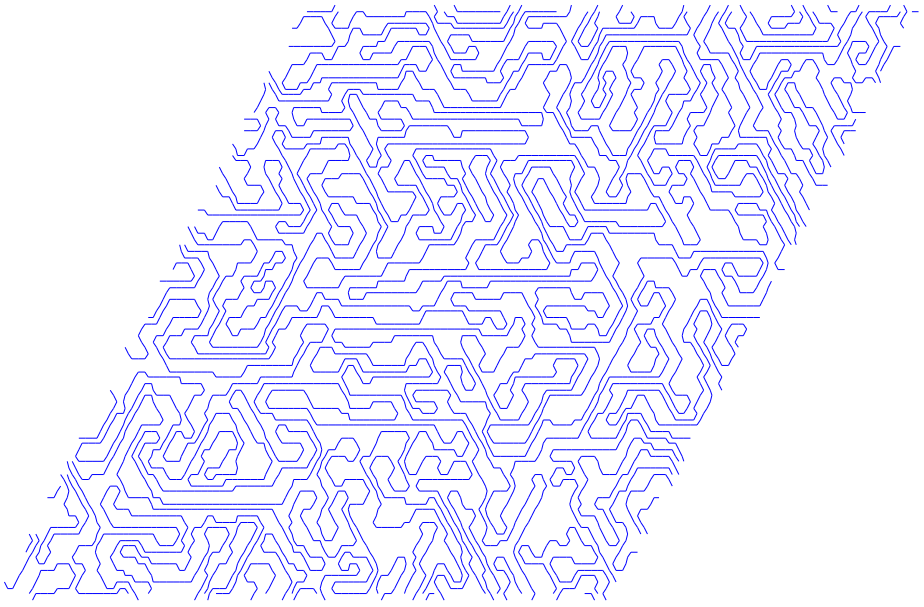

Figure 15. The $1:\infty$ model in equilibrium at $\mu = -0.4$

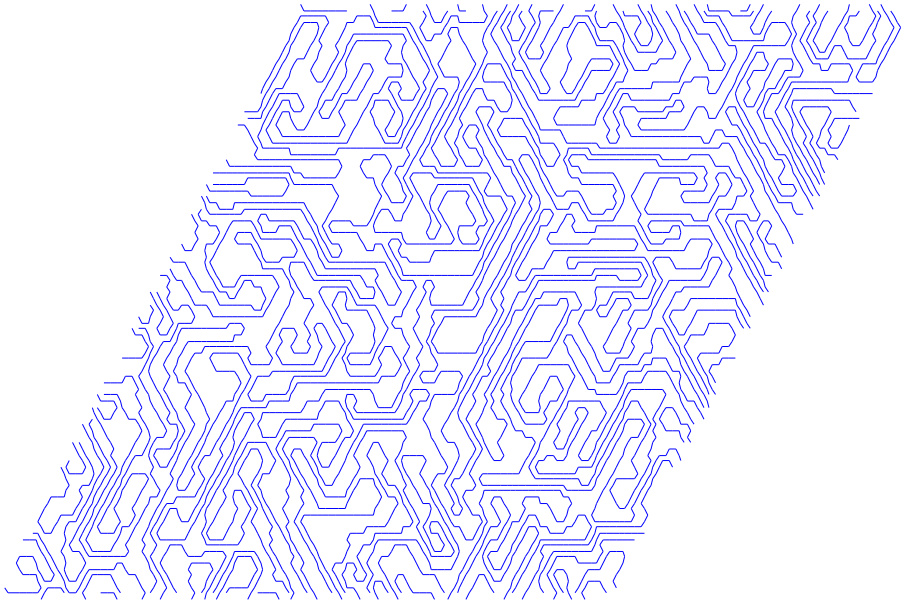

Figure 16. The $1:\infty$ model in equilibrium at $\mu = -0.3$

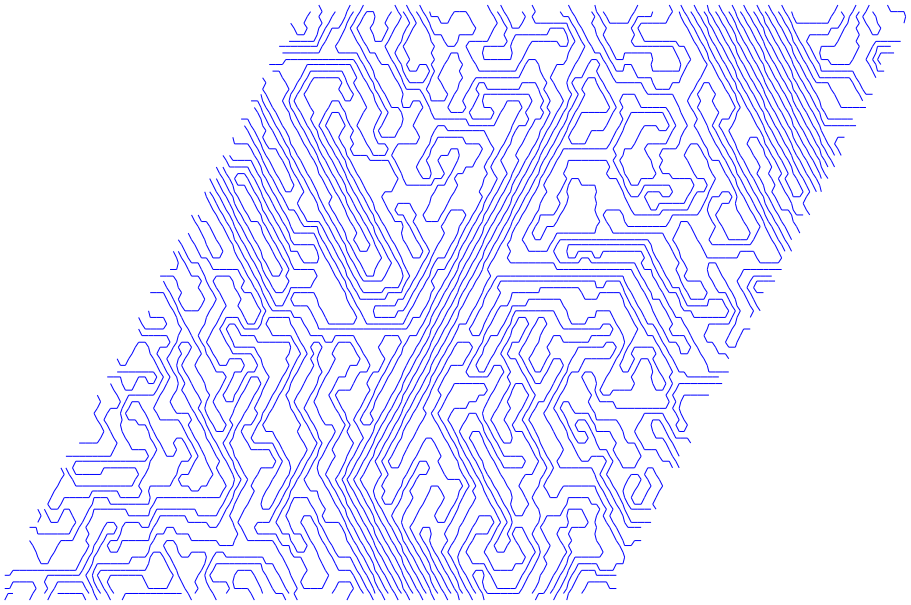

Figure 17. The $1:\infty$ model in equilibrium at $\mu = -0.2$

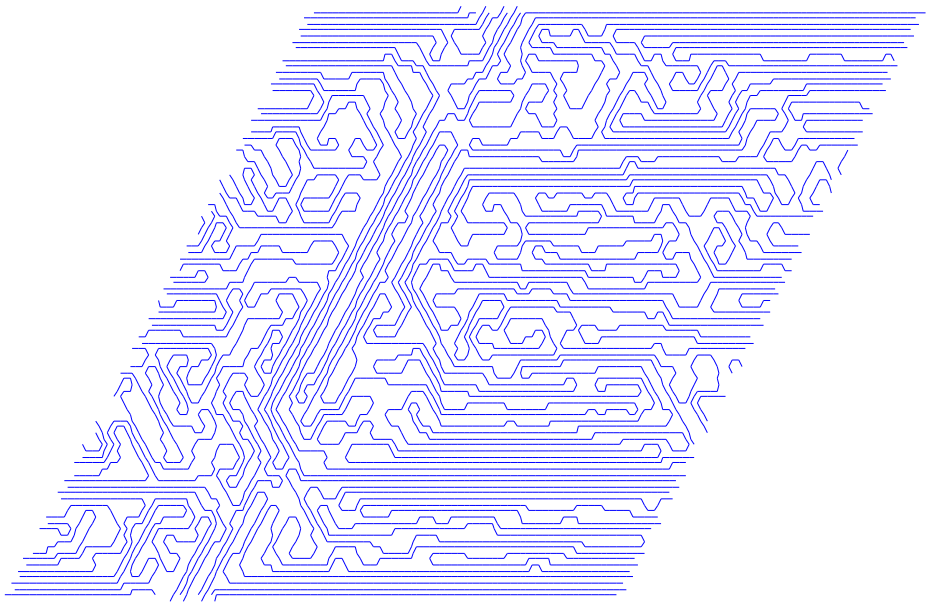

Figure 18. The $1:\infty$ model in equilibrium at $\mu = -0.1$

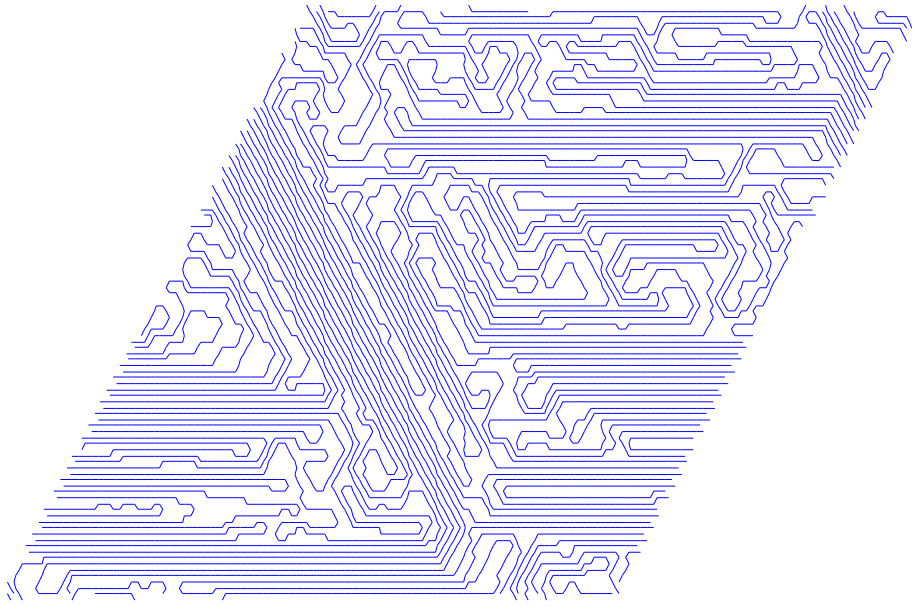

Figure 19 The $1:\infty$ model in equilibrium at $\mu = 0.0$.

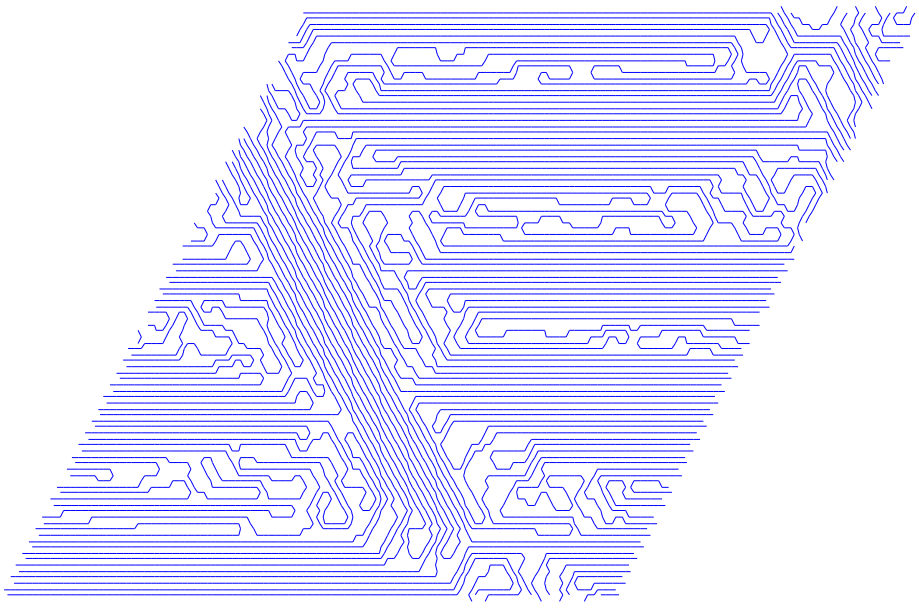

Figure 20 The $1:\infty$ model in equilibrium at $\mu = 0.1$.

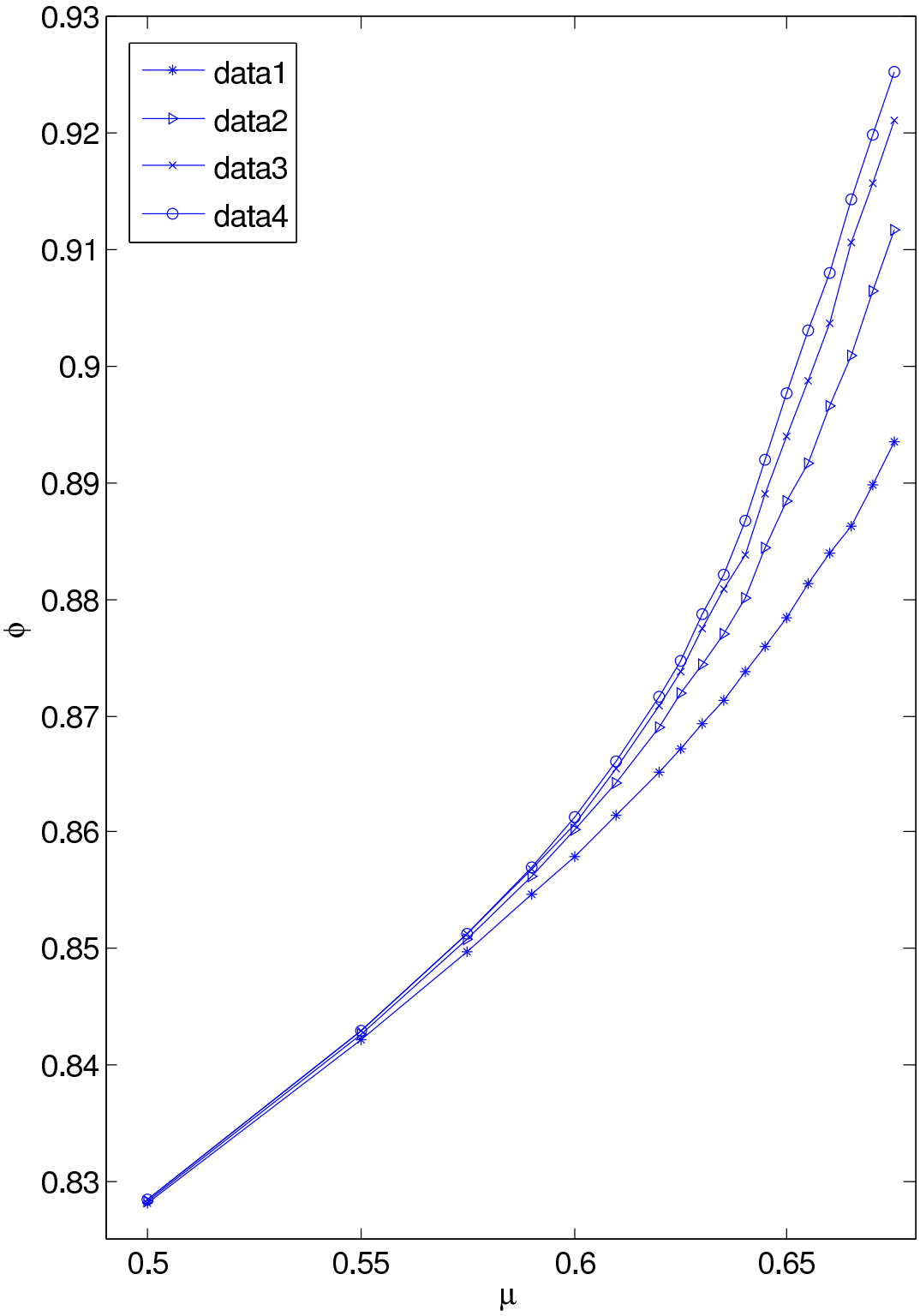

Figure 21. Volume fraction vs. mu for the 1 : 2 model, for volumes 40^2 (data1) through 100^2 (data4).

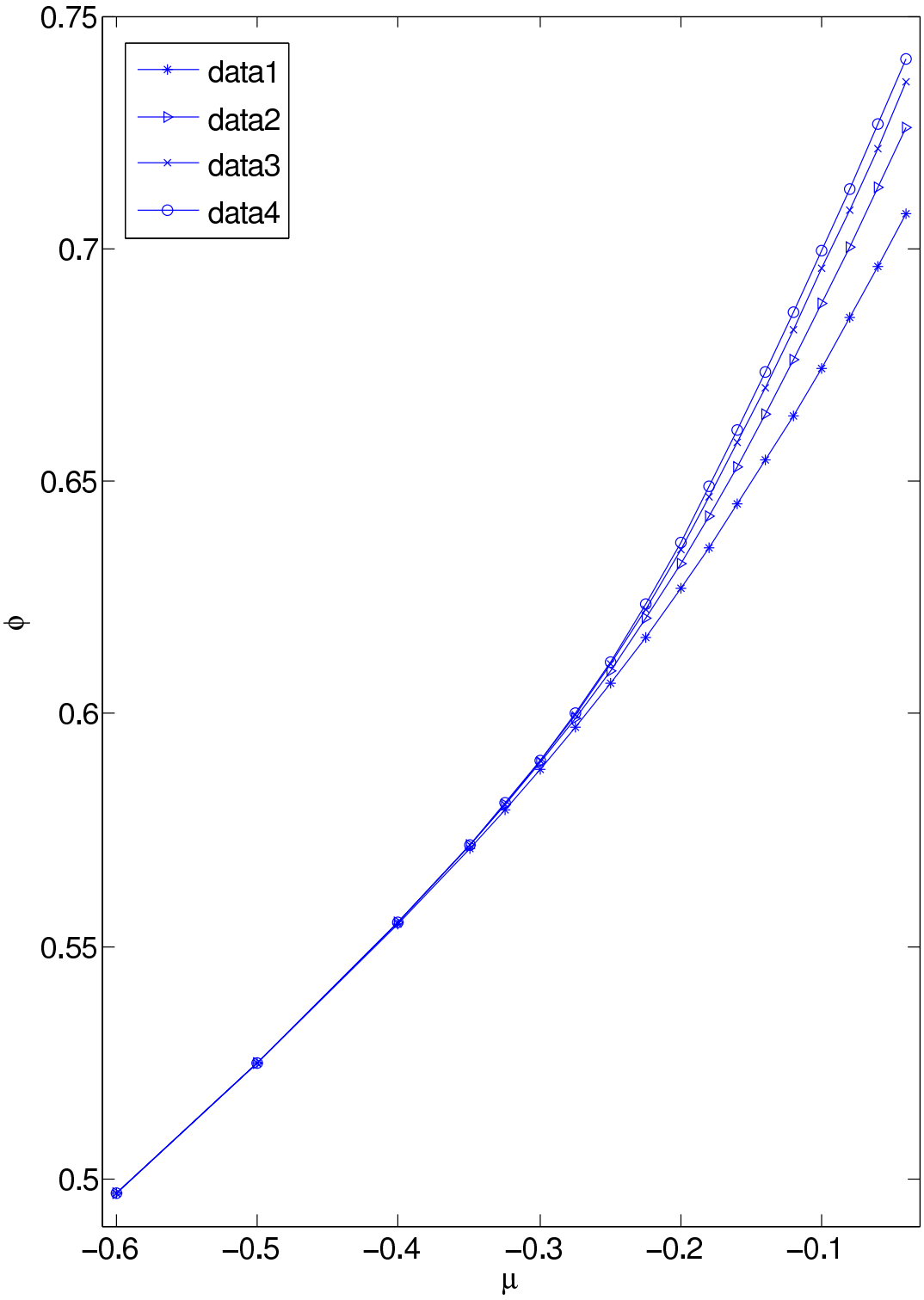

Figure 22. Volume fraction vs. mu for the $1 : \infty$ model, for volumes 40^2 (data1) through 100^2 (data4).

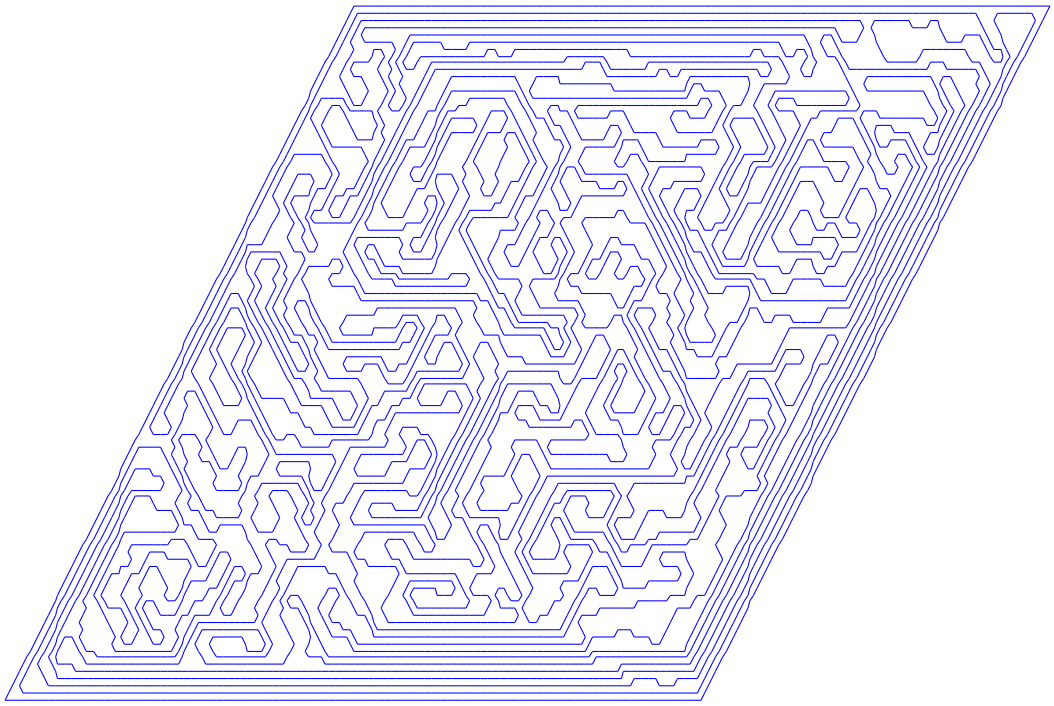

Figure 23. A configuration in equilibrium at $\mu = -0.2$, with flat boundary

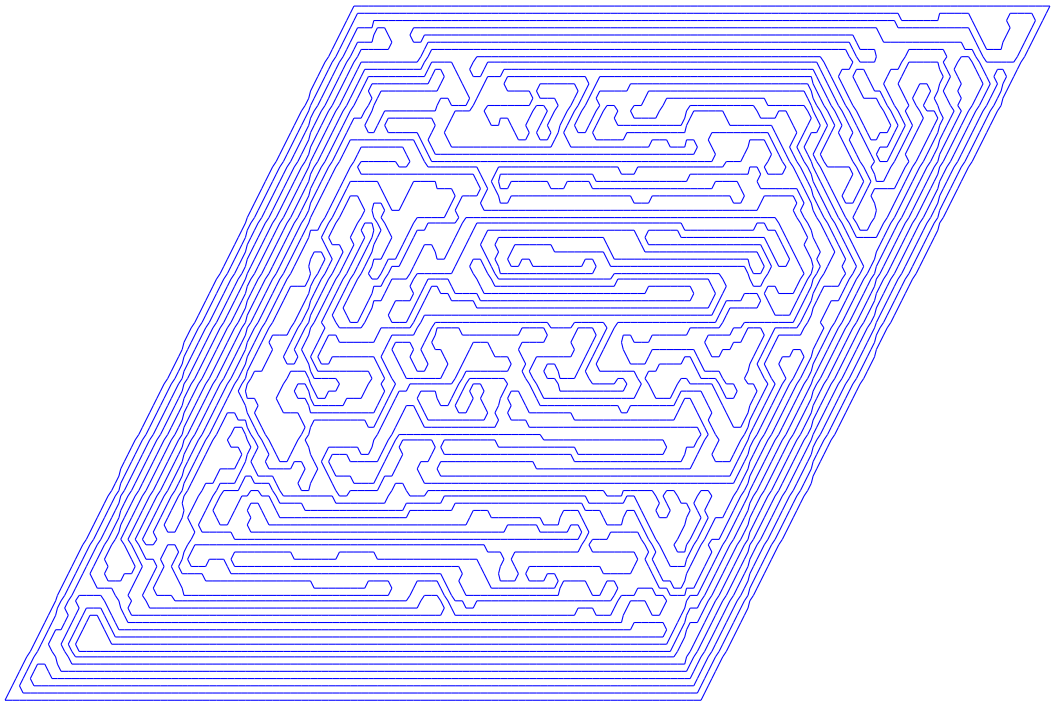

Figure 24. A configuration in equilibrium at $\mu = 0$, with flat boundary

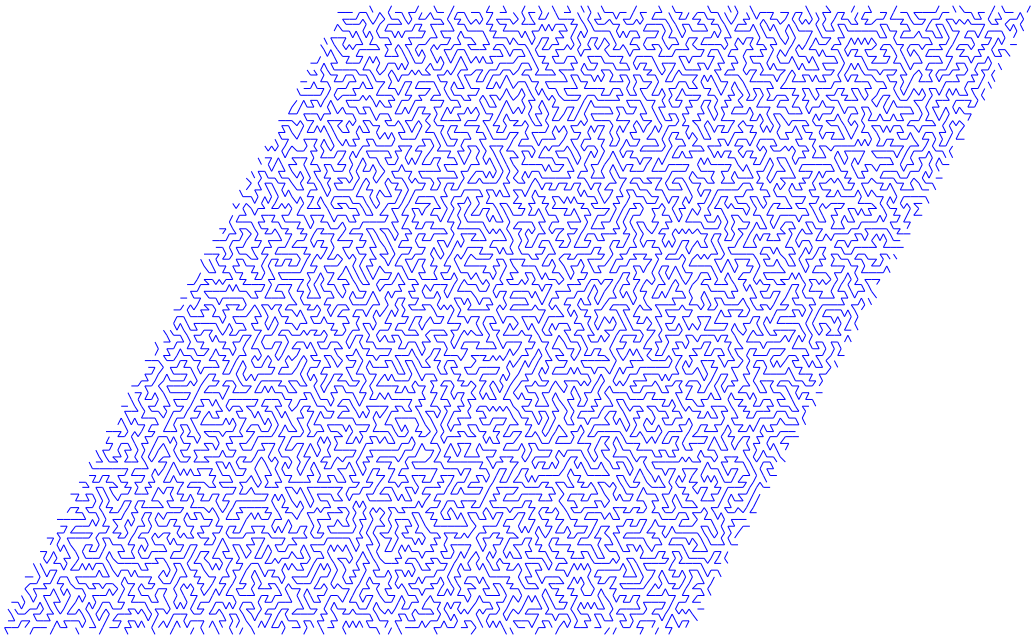

Figure 25. A typical configuration at volume fraction 0.9977, with no cost for a bend.

References

[1] T.A. Witten, Stress focusing in elastic sheets, R. Mod. Phys., 79 (2007), 643-675.

[2] K. Matan, R.B. Williams, T.A. Witten and S.R. Nagel, Crumpling a thin sheet, Phys. Rev. Let. 88, No. 7 (2002) 076101.

[3] A.S. Balankin and O.S. Huerta, Entropic rigidity of a crympling network in a randomly folded thin sheet, Phys. Rev. E 77 (2008) 051124.

[4] Y. Kantor, Properties of tethered surfaces, in "Statistical Mechanics of Membranes and Surfaces - Proceedings of the Fifth Jerusalem Winter School for Theoretical Physics", ed. by D. R. Nelson, T. Piran and S. Weinberg, World Scientific, Singapore, (1989) pp. 115-136.

[5] A. Sultan and A. Boudaoud, Statistics of crumpled paper, Phys. Rev. Let. 96 (2006) 136103.

[6] Y.C.Lin, Y.W. Lin and T.M. Hong, Crumpling wires in two dimensions, Phys. Rev. E 78 (2008) 067101.

[7] M.E.J. Newman and G.T. Barkema, Monte Carlo Methods in Statistical Physics, Oxford University Press (1999).

[8] W. Krauth, Statistical Mechanics: Algorithms and Computations (Oxford Master Series in Statistical, Computational, and Theoretical Physics), Oxford University Press (2006).

[9] E.J. Rensburg, Monte Carlo methods for the self-avoiding walk, J. Phys. A 42 (1992) 323001.

[10] C.J. Geyer, Practical Markov chain Monte Carlo, Stat. Sci. 7 (1992) 473-483.

[11] M.A. Rutgers, J.H. Dunsmuir, J.-Z. Xue, W.B. Russel and P.M. Chaikin, Measurement of the hard-sphere equation of state using screened charged polystyrene colloids, Phys. Rev. B 53 (1996) 5043-5046.

[12] C. Radin, Random close packing of granular matter, J. Stat. Phys. 131(2008), 567-573.

[13] D. Aristoff and C. Radin, Random close packing in a granular model, arXiv:0909.2608.